An MSK Waveform for Radar Applications

Kevin J. Quirk and Meera Srinivasan
Jet Propulsion Laboratory
California Institute of Technology
Pasadena, CA, 91109, USA

***Abstract*— We introduce a minimum shift keying (MSK) waveform developed for use in radar applications. This waveform is characterized in terms of its spectrum, autocorrelation, and ambiguity function, and is compared with the conventionally used bi-phase coded (BPC) radar signal. It is shown that the MSK waveform has several advantages when compared with the BPC waveform, and is a better candidate for deep-space radar imaging systems such as NASA's Goldstone Solar System Radar.**

I. Introduction

The Goldstone Solar System Radar (GSSR) is an instrument within NASA's Deep Space Network (DSN) that is used by scientists to investigate astronomical bodies within the solar system; this includes planets, moons, asteroids, and debris orbiting the earth. Measurements of a body's ephemerides, dynamics, topography, and composition are enabled through the use of Radio Detection and Ranging (RADAR). Currently, the GSSR uses a bi-phase coded (BPC) radar waveform in which a pseudo-noise (PN) sequence is used to rotate the phase of a sinusoid between two phase offsets 180 degrees apart, and from which measurements of amplitude, Doppler, polarization, and range of the returned echoes may be processed. The BPC waveform, with its discontinuous phase and large spectral sidelobes, is limited to a mainlobe of $16MHz$ due to transmit amplifier constraints, providing a maximum range resolution of $18.75m$. Digital elevation maps (DEM) with resolutions finer than this will require the introduction of a new radar waveform.

In this article, we introduce a new minimum-shift-keying (MSK) type of radar waveform as a continuous-phase alternative to the BPC signal. We start by discussing the conventially used BPC waveform, and then introduce the MSK radar waveformand derive its autocorrelation function, spectrum, and ambiguity function, which indicate the achievable Doppler and range resolutions. It is shown that ideal auto and crosscorrelation properties may be obtained for the MSK waveform through use of a specific configuration of modulating PN sequences. Finally, quantitative comparisons are made between the characteristics of the two signals, using the example of a lunar imaging application to demonstrate the advantages of the MSK waveform for radar applications.

II. Bi-phase Coded (BPC) Waveform

A BPC waveform is constructed from a pseudonoise (PN) sequence by switching the waveform to plus or minus one, every T_c seconds. The transmitted signal, $x(t)$, is formed by periodically extending the BPC waveform and modulating it onto a radio frequency (RF) carrier with a frequency ω_c. Writing this in terms of the baseband signal, we have

$$z(t) = \Re\left\{\sum_{k=-\infty}^{\infty} x(t-kMT_c)e^{j\omega_c t}\right\}, \tag{1}$$

where

$$x(t) = \sum_{n=0}^{M-1} c_n p(t-nT_c), \tag{2}$$

$\{c_n\}$ represents the elements of the PN sequence of length M, and $p(t)$ is a rectangular pulse of duration T_c. As the waveform is periodically extended, the use of an m-sequence [1], with its circular properties, for the PN sequence will result in a uniform autocorrelation sidelobe level. The waveform has a discontinuous phase which, with bandlimiting, will result in a non-constant envelope, leading to potential degradation from AM to PM conversion in a transmit power amplifier operating in saturation [2, pp 203-209].

A. Autocorrelation

The radar signal autocorrelation function indicates the maximum achievable delay resolution. The autocorrelation function of $z(t)$ is periodic, with a single period given by

$$\begin{aligned} r(\tau) &= \frac{1}{MT_c}\int_{-MT_c/2}^{MT_c/2} z(t)z(t+\tau)dt \\ &= \frac{1}{2}\Re\left\{\tilde{r}(\tau)e^{j\omega_c\tau}\right\} \quad -MT_c/2 \le \tau \le MT_c/2. \end{aligned} \tag{3}$$

The autocorrelation of the complex baseband signal, $\tilde{r}(\tau)$, assuming the use of an m-sequence [1] for the PN sequence, is

$$\tilde{r}(\tau) = \begin{cases} 1-\frac{M+1}{M}\frac{\tau}{T_c} & |\tau| < T_c \\ -\frac{1}{M} & |\tau| \ge T_c \end{cases}. \tag{4}$$

Using the $6dB$ extent of the autocorrelation as a measure of the delay resolution, we have, for the BPC waveform,

$$\Delta_{6dB} = T_c. \tag{5}$$

B. Spectrum

The power spectral density (PSD) of the BPC waveform is given by

$$S(\omega) = \frac{1}{4}S_c(\omega-\omega_c) + \frac{1}{4}S_c^*(-\omega-\omega_c), \tag{6}$$

where

$$S_c(\omega) = \frac{2\pi}{M^2}\delta(\omega) + 2\pi\frac{M+1}{M^2}\sum_{\substack{n=-\infty \\ n\neq 0}}^{\infty} \frac{\sin^2\left(\frac{\pi n}{M}\right)}{\left(\frac{\pi n}{M}\right)^2}\delta\left(\omega - \frac{n2\pi}{MT_c}\right). \tag{7}$$

The spectrum is composed of spectral lines spaced at harmonics of the waveform repetition rate. As the period of the waveform increases, the spacing of the harmonics becomes closer, and their associated power decreases; the total power is constant. The mainlobe bandwidth of the waveform is $B = 2/T_c$ Hz.

C. Ambiguity Function

The radar waveform ambiguity function determines the fidelity of the range and Doppler measurements. The ambiguity function of a signal with period T is defined as

$$\xi(\tau, f_d) \triangleq \frac{1}{T}\int_{-T/2}^{T/2} z(t)z(t+\tau)e^{j2\pi f_d t}dt \qquad -T/2 \leq \tau < T/2. \tag{8}$$

Evaluating this with (1), and letting $\tau = lT_c + \hat{\tau}$, we have

$$\xi(l, \hat{\tau}, f_d) = \frac{1}{2}\Re\left\{e^{j\omega_c\tau}\tilde{\xi}(l, \hat{\tau}, f_d)\right\} \qquad -T/2 \leq \tau < T/2, \tag{9}$$

where

$$\begin{aligned}\tilde{\xi}(l, \hat{\tau}, f_d) &= \frac{e^{-j\pi f_d\hat{\tau}}}{MT_c}\frac{\sin(\pi f_d\hat{\tau})}{\pi f_d}\sum_{n=0}^{M-1} c_n c_{n+1+l}e^{j2\pi f_d(n+1)T_c} \\ &+ \frac{e^{-j\pi f_d(T_c-\hat{\tau})}}{MT_c}\frac{\sin(\pi f_d(T_c-\hat{\tau}))}{\pi f_d}\sum_{n=0}^{M-1} c_n c_{n+l}e^{j2\pi f_d nT_c}. \end{aligned} \tag{10}$$

Defining the effective Doppler domain as the $1dB$ extent of the ambiguity function on the Doppler axis at $\tau = 0$, one can show that $\tilde{\xi}$ is dominated by the term $\frac{\sin(\pi f_d MT_c)}{\pi f_d MT_c}$ for $f_d << M/T$, and that Doppler shifts within $-\frac{1}{4MT_c} \leq f_d \leq \frac{1}{4MT_c}$ are detectable. Relating this to the bandpass signal, the effective Doppler Bandwidth is

$$B_{D_{eff}} = \frac{1}{2MT_c}. \tag{11}$$

Another important characteristic of the ambiguity function is the peak ambiguity sidelobe, which must be low enough to suppress backscatter from pixels near the target. To find the peak ambiguity function sidelobe, in delay and Doppler, we approximate the magnitude square of the complex baseband ambiguity function as

$$\begin{aligned}|\tilde{\xi}(l, \hat{\tau}, f_d)|^2 &\approx \frac{(M+1)}{M^2T_c^2}\hat{\tau}^2 + \frac{(M+1)}{M^2T_c^2}(T_c-\hat{\tau})^2 \\ &+ \frac{2(M+1)}{M^2T_c^2}\hat{\tau}(T_c-\hat{\tau}), \end{aligned} \tag{12}$$

which is maximized at $\hat{\tau} = T_c/2$ with value

$$\xi_{peak} = \frac{1}{\sqrt{M}} = \sqrt{\frac{2}{BT}}. \tag{13}$$

III. Minimum-shift-keying (MSK) Waveform

Our proposed alternative to the BPC waveform is a new MSK radar signal that is formed by periodically extending a waveform that separately modulates the in-phase and quadrature-phase components of the carrier with offset pulse-shaped PN sequences. To generate this waveform, a pair of periodic PN sequences, $\{c_n^{(i)}\}$ and $\{c_n^{(q)}\}$, are each passed through a pulse shaping filter with a half sinusoid impulse response, $s(t)$. These shaped PN waveforms are then offset by half a chip time, $T_c/2$, and separately modulated on the in-phase and quadrature phase components of an RF carrier as shown in Figure 1. Writing the transmitted signal $z(t)$ in terms of the baseband signal, we have

$$z(t) = \Re\left\{\sum_{k=-\infty}^{\infty} x(t-kMT_c)e^{j\omega_c t}\right\}, \tag{14}$$

where

$$x(t) = \sum_{n=0}^{M-1} c_n^{(i)} s\left(t - nT_c + \frac{T_c}{2}\right) - j\sum_{m=0}^{M-1} c_m^{(q)} s(t - mT_c), \tag{15}$$

$$s(t) = \begin{cases} \sin\left(\frac{\pi t}{T_c}\right) & 0 \leq t < T_c \\ 0 & otherwise \end{cases}, \tag{16}$$

and M is the period of the PN sequences. By writing the signal in a magnitude phase form it can be shown to have a constant envelope and to have a continuous phase that varies linearly by $\pm\frac{\pi}{2}$ radians each $T_c/2$ interval. We also note that the frequency of the waveform changes by $\pm\frac{\pi}{T_c}$ every $T_c/2$ and can thus be viewed as a minimum shift keying (MSK) type waveform; this is a well-known property of this type of shaped offset quadrature phase shift keying waveforms.

A. Autocorrelation

The autocorrelation function of $z(t)$ is periodic; a single period is given by

$$\begin{aligned} r(\tau) &= \frac{1}{MT_c}\int_{-MT_c/2}^{MT_c/2} z(t)z(t+\tau)dt \\ &= \frac{1}{2}\Re\left\{\tilde{r}(\tau)e^{j\omega_c\tau}\right\} \quad -MT_c/2 \leq |\tau| < MT_c/2, \end{aligned}$$

where $\tilde{r}(\tau)$ is the autocorrelation of the complex baseband signal. Letting $\tau = lT_c + \hat{\tau}$, where $l = \lfloor\frac{\tau}{T_c}\rfloor$ and $\hat{\tau} = \tau - lT_c$, we have

$$\tilde{r}(l, \hat{\tau}) = \begin{cases} \frac{\alpha_l}{M}\rho(T_c-\hat{\tau}) + \frac{\alpha_{l+1}}{M}\rho(\hat{\tau}) + \frac{j}{2M}\left[(\beta_{l-1}-\beta_{-l})\rho\left(\frac{T_c}{2}-\hat{\tau}\right)\right. & \\ \left.+(\beta_l-\beta_{-l-1})\rho\left(\frac{T_c}{2}+\hat{\tau}\right)\right], & 0 \leq \hat{\tau} < \frac{T_c}{2} \\ \frac{\alpha_l}{M}\rho(T_c-\hat{\tau}) + \frac{\alpha_{l+1}}{M}\rho(\hat{\tau}) + \frac{j}{2M}\left[(\beta_l-\beta_{-l-1})\rho\left(\frac{3T_c}{2}-\hat{\tau}\right)\right. & \\ \left.+(\beta_{l+1}-\beta_{-l-2})\rho\left(\hat{\tau}-\frac{T_c}{2}\right)\right], & \frac{T_c}{2} \leq \hat{\tau} < T_c \end{cases} \tag{17}$$

where

$$\rho(\tau) \triangleq -\cos\left(\frac{\pi\tau}{T_c}\right)\frac{\tau}{T_c} + \frac{1}{\pi}\sin\left(\frac{\pi\tau}{T_c}\right), \tag{18}$$

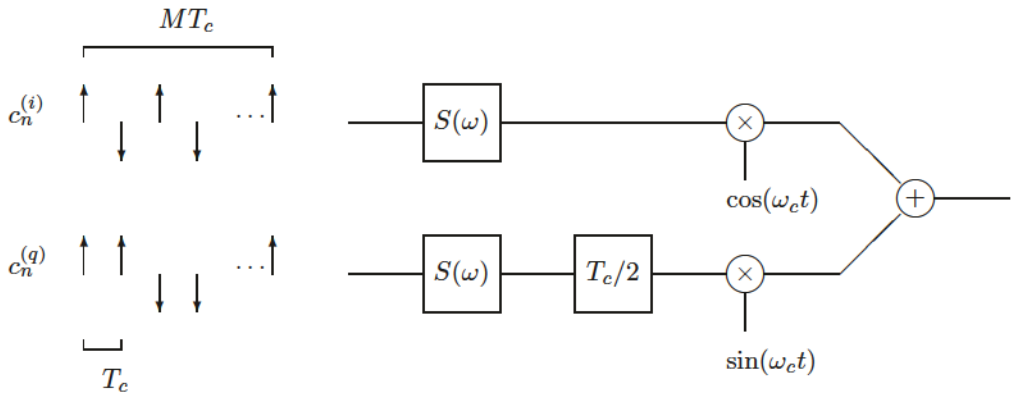

Fig. 1. MSK waveform generation, with a chip time T_c and a duration MT_c.

$$\alpha_k \triangleq \sum_{n=0}^{M-1} c_n^{(i)} c_{n+k}^{(i)}, \tag{19}$$

and

$$\beta_k \triangleq \sum_{n=0}^{M-1} c_n^{(i)} c_{n+k}^{(q)}. \tag{20}$$

The autocorrelation functions of the in-phase and quadrature-phase sequences are assumed to be identical, $\alpha_k^{(i)} = \alpha_k^{(q)}$, and the cross-correlation between the in-phase and quadrature-phase sequences satisfies $\beta_k^{(i,q)} = \beta_{-k}^{(q,i)}$.

The autocorrelation has a mainlobe, extending from $[-T_c, T_c]$, dominated by

$$\tilde{r}(l,\hat{\tau}) \approx -\cos\left(\frac{\pi}{T_c}(T_c - |\hat{\tau}|)\right)\frac{T_c - |\hat{\tau}|}{T_c} + \frac{1}{\pi}\sin\left(\frac{\pi}{T_c}(T_c - |\hat{\tau}|)\right) \quad \text{for} \quad l = -1, 0 \quad |\hat{\tau}| \le T_c.$$

This function has a peak value at $\hat{\tau} = 0$, is zero at $\hat{\tau} = \pm T_c$, and has a cosine response near $\hat{\tau} = 0$, giving way to a more rapid decay as $|\hat{\tau}|$ increases. The delay resolution, given as the $6dB$ extent of the mainlobe of the autocorrelation, is

$$\Delta_{6dB} = 0.8T_c. \tag{21}$$

The magnitude square of the autocorrelation function of the complex baseband signal, $\tilde{r}(\tau)$, for delays less than $\pm T_c$ is plotted in Figure 2. Note the slow roll-off near $\tau = 0$ gives way to a rapid decay, reaching the $6dB$ level at $\tau = 0.4T_c$. The autocorrelation of a BPC waveform with an equal chip time, T_c, is also shown. Comparing the two waveforms, the autocorrelation of the MSK waveform exceeds that of the BPC for small τ and drops off more rapidly beyond the delay resolution.

The peak sidelobe levels of the autocorrelation, (17), are dependent on both the autocorrelations and cross correlation of the PN sequences; the proper choice of these sequences is vital. One option is to use a preferred pair of m-sequences [1]. In that case, for the region outside the mainlobe, $|\tau| > T_c$, the cross-correlation terms will dominate and local maxima will occur at odd multiples of half the chip time such that

$$|\tilde{r}(\tau)| \le \frac{2^{\frac{e}{2}}\sqrt{M+1}}{M} \qquad |\tau| \ge T_c. \tag{22}$$

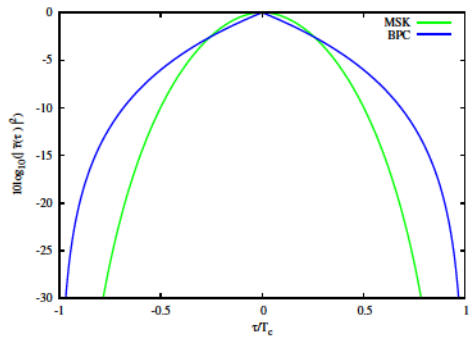

Fig. 2. Autocorrelation of a complex baseband MSK waveform and a complex baseband BPC waveform for $|\tau| < T_c$.

Here, $e = 1$ when $n = \log_2(M+1)$ is odd, and $e = 2$ when $n = \log_2(M+1)$ is even.

Another option to generate the two sequences is to use offset periods of a single m-sequence. For the in-phase channel use the m-sequence with no offset into the code sequence, and on the quadrature channel use the m-sequence offset by a fraction of the period. In this case, the auto and cross-correlation functions of the sequences will be two valued:

$$\alpha_k = \begin{cases} M & k \bmod M = 0 \\ -1 & \text{otherwise} \end{cases}, \tag{23}$$

$$\beta_k = \begin{cases} M & k = K \bmod M \\ -1 & \text{otherwise} \end{cases}, \tag{24}$$

where K is the offset into the sequence for the quadrature channel, i.e., $c_k^{(q)} = c_{k-K}^{(i)}$. We can then select the offset K to optimize the autocorrelation function by considering the region outside the mainlobe, $|\tau| > T_c$, where the cross-correlation between the two sequences dominates the auto-correlation. In particular, if we let $K = \frac{M-1}{2}$, then the peak cross-correlation terms are eliminated, and the autocorrelation of the complex baseband waveform becomes

$$\tilde{r}(l,\hat{\tau}) \quad = \quad \frac{\alpha_l}{M}\rho(T_c - \hat{\tau}) + \frac{\alpha_{l+1}}{M}\rho(\hat{\tau}). \tag{25}$$

For $|\tau| > T_c$ the sidelobe structure will have local maxima occurring at integer multiples of T_c, with peak sidelobe values

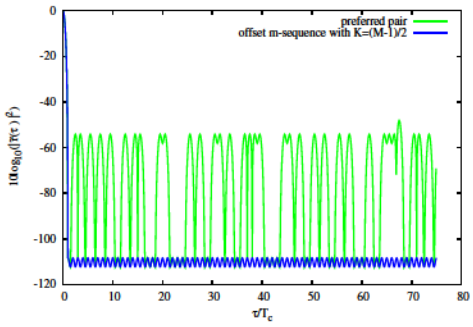

Fig. 3. Autocorrelation of a complex baseband MSK waveform using a preferred pair of m-sequences, as well as that of a complex baseband MSK waveform generated using a single m-sequence with an offset period of $K = \frac{M-1}{2}$, where $M = 2^{18} - 1$.

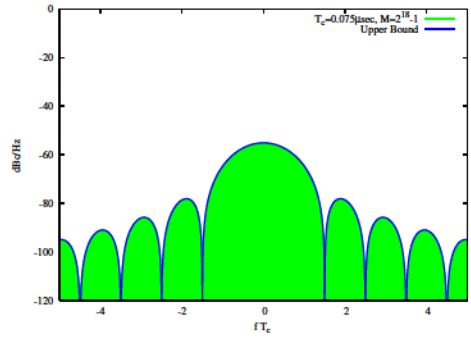

Fig. 4. The spectral power in $1Hz$ intervals for an MSK waveform with $T_c = 0.075\mu sec$ and $M = 2^{18} - 1$.

given by

$$\tilde{r}(l, T_c) = -\frac{1}{M}, \tag{26}$$

and local minima at odd integer multiples of $T_c/2$ with values

$$\tilde{r}\left(l, \frac{T_c}{2}\right) = -\frac{2}{M\pi}. \tag{27}$$

The use of a pair of codes, generated from a single m-sequence with a code offset of $\frac{M-1}{2}$ between the in-phase and quadrature-phase, can thus achieve both ideal auto and cross correlation properties when used in this configuration. Figure 3 shows the magnitude square of the complex baseband autocorrelation using the offset codes, as well as that obtained by using a preferred pair of m-sequences.

B. Spectrum

The power spectral density of the MSK waveform is found by representing the periodic waveform in terms of its Fourier series, solving for the autocorrelation, and then taking the Fourier transform to obtain

$$S(\omega) = \frac{1}{4}F(\omega - \omega_c) + \frac{1}{4}F^*(-\omega - \omega_c), \tag{28}$$

where

$$F(\omega) = \sum_{k=-\infty}^{\infty} |a_k|^2 2\pi\delta\left(\omega + \frac{2\pi}{MT_c}k\right) \tag{29}$$

with

$$|a_k|^2 = \frac{4}{M^2\pi^2}\frac{\cos^2\left(\frac{\pi k}{M}\right)}{\left(1 - \left(\frac{2k}{M}\right)^2\right)^2} \left| e^{j\frac{\pi k}{M}} \sum_{n=0}^{M-1} c_n^{(i)} e^{-j\frac{2\pi}{M}nk} - j\sum_{m=0}^{M-1} c_m^{(q)} e^{-j\frac{2\pi}{M}mk} \right|^2. \tag{30}$$

Using Parseval's relation, an upper bound to $|a_k|^2$ can be obtained, giving

$$|a_k|^2 \leq \begin{cases} 2 & k = 0 \\ 2(M+1) & k = \pm 1, \pm 2, \cdots \end{cases}. \tag{31}$$

The spectrum is composed of spectral lines spaced at harmonics of the waveform repetition rate. As the period of the waveform increases, the spacing of these harmonics becomes closer, and their associated power decreases. The mainlobe bandwidth of the waveform is $B = \frac{3}{T_c}$ Hz, and the spectral sidelobes decay more quickly than those of a corresponding BPC waveform.

Figure 4 contains a plot of the power of the waveform in $1Hz$ increments for a signal with a period $M = 2^{18} - 1$ using the m-sequence formed by the linear feedback shift register $0x40081$, and a chip time $T_c = 0.075\mu sec$; the curve formed from the PSD and a curve formed from the bound (31) are shown. The mainlobe bandwidth is $B = \frac{3}{T_c} = 40MHz$.

C. Ambiguity Function

The ambiguity function of the MSK waveform, assuming the code sequences $\{c_n^{(i)}\}$ and $\{c_n^{(q)}\}$ are generated from a single m-sequence with a period offset of $K = \frac{M-1}{2}$ and $f_d << \frac{\sqrt{M}}{T}$, is given by

$$\xi(l, \hat{\tau}, f_d) = \frac{1}{2}\Re\left\{\tilde{\xi}(l, \hat{\tau}, f_d)e^{j\omega_c\tau}\right\} \qquad -T/2 \leq \tau < T/2,$$

where

$$\tilde{\xi}(l, \hat{\tau}, f_d) = \frac{e^{-j\pi f_d\hat{\tau}}}{2M}\Big[\gamma(T_c - \hat{\tau}, f_d)\,\alpha_l^{(i)} + \gamma(\hat{\tau}, f_d)\,e^{j\pi f_d T_c}\alpha_{l+1}^{(i)} + \gamma(T_c - \hat{\tau}, f_d)\,e^{j\pi f_d T_c}\alpha_l^{(q)} + \gamma(\hat{\tau}, f_d)\,e^{j\pi f_d 2T_c}\alpha_{l+1}^{(q)}\Big]$$
$$\text{for} \qquad 0 \leq \hat{\tau} < T_c, \qquad l \in \left[-\frac{M}{2}, \frac{M}{2}\right), \tag{32}$$

with

$$\gamma(\tau, f_d) \triangleq \begin{cases} -\frac{\cos\left(\frac{\pi}{T_c}\tau\right)\sin(\pi f_d\tau)}{\pi f_d T_c} + \frac{\sin\left(\pi\left(\frac{1}{T_c}+f_d\right)\tau\right)}{2\pi\left(\frac{1}{T_c}+f_d\right)T_c} + \frac{\sin\left(\pi\left(-\frac{1}{T_c}+f_d\right)\tau\right)}{2\pi\left(-\frac{1}{T_c}+f_d\right)T_c} & f_d \neq 0 \\ -\cos\left(\frac{\pi\tau}{T_c}\right)\frac{\tau}{T_c} + \frac{1}{\pi}\sin\left(\frac{\pi\tau}{T_c}\right) & f_d = 0 \end{cases} \tag{33}$$

and

$$\alpha_k^{(i)} \triangleq \sum_{n=0}^{M-1} c_n^{(i)} c_{n+k}^{(i)} e^{j2\pi f_d T_c n}, \qquad \alpha_k^{(q)} \triangleq \sum_{n=0}^{M-1} c_n^{(q)} c_{n+k}^{(q)} e^{j2\pi f_d T_c n}.$$

To determine the domain of Doppler offsets that can be effectively detected, we consider the $1dB$ extent of the

ambiguity function on the Doppler axis at $\tau = 0$. Setting $\hat{\tau} = 0$ and $l = 0$, the ambiguity function reduces to

$$\tilde{\xi}(0,0,f_d) \approx e^{j\pi f_d T_c (M-\frac{1}{2})} \cos\left(\pi \frac{f_d T_c}{2}\right) \frac{\sin(\pi f_d M T_c)}{\pi f_d M T_c} \times \left[\frac{\sin(\pi f_d T_c)}{\pi f_d T_c} + \frac{\sin(\pi(f_d T_c + 1))}{2\pi(f_d T_c + 1)} + \frac{\sin(\pi(f_d T_c - 1))}{2\pi(f_d T_c - 1)}\right]. \quad (34)$$

For $f_d << \frac{M}{T}$, the $sin(x)/x$ response with the first null occurring at $f_d = 1/(MT_c)$ dominates. Using the $1dB$ extent of the mainlobe as the the effective Doppler domain, Doppler shifts within

$$-\frac{1}{4MT_c} \leq f_d \leq \frac{1}{4MT_c} \quad (35)$$

are detectable. As with the BPC waveform, the effective Doppler Bandwidth is

$$B_{D_{eff}} = \frac{1}{2MT_c}. \quad (36)$$

To find the peak ambiguity function sidelobe, in delay and Doppler, we take the magnitude of the complex baseband ambiguity function evaluated at $\hat{\tau} = T_c$:

$$\begin{aligned} |\tilde{\xi}(l,T_c,f_d)| &= \frac{1}{2M}\Big|\gamma(0,f_d)\left(\alpha_l^{(i)} + e^{j\pi f_d T_c}\alpha_l^{(q)}\right) \\ &\quad + \gamma(T_c,f_d)\left(e^{j\pi f_d T_c}\alpha_{l+1}^{(i)} + e^{j\pi f_d 2T_c}\alpha_{l+1}^{(q)}\right)\Big| \\ &\leq \frac{1}{2M}\left|\left(\alpha_l^{(i)} + e^{j\pi f_d T_c}\alpha_l^{(q)}\right)\right|. \end{aligned} \quad (37)$$

For the region outside the mainlobe, $l \neq \{-1,0,1\}$ and $f_d \neq 0$, it can be shown, using Parseval's relation, that for an m-sequence, $\{c_n\}$,

$$\left|\sum_{n=0}^{M-1} c_n c_{n+1+l} e^{j2\pi f_d (n+1) T_c}\right|^2 \approx M + 1. \quad (38)$$

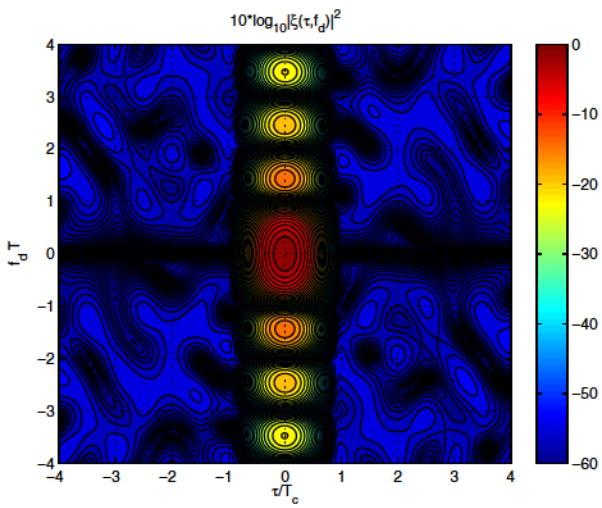

Fig. 5. Contour plot of the ambiguity function of the complex baseband MSK waveform, generated using a single m-sequence of length $M = 2^{18} - 1$ with offset $K = 0$ for the in-phase and $K = \frac{M-1}{2}$ for the quadrature-phase sequence, encompassing the mainlobe.

Applying this approximation, we have

$$|\tilde{\xi}(l,T_c,f_d)| \leq \frac{1}{2M}\sqrt{\left|\alpha_l^{(i)} + e^{j\pi f_d T_c}\alpha_l^{(q)}\right|^2} = \sqrt{\frac{M+1}{M^2}} \approx \frac{1}{\sqrt{M}}.$$

The peak ambiguity function sidelobe is therefore given by

$$\xi_{peak} = \frac{1}{\sqrt{M}} = \sqrt{\frac{3}{BT}}. \quad (39)$$

The magnitude square of the ambiguity function of the complex baseband signal is plotted in Figure 5 for the MSK waveform with $T_c = 0.075\mu sec$ and a code period $M = 2^{18} - 1$ generated from the linear feedback shift register $0x40081$. In Figure 5, a domain encompassing the mainlobe is shown in order to demonstrate the mainlobe and peak sidelobe structure of the function. Considering the mainlobe, the delay resolution of $\Delta_{6dB} = 0.8T_c$ is evident along with the effective Doppler resolution of $B_{D_{eff}} = \frac{1}{2T}$. Outside of the mainlobe, the peak sidelobes of $-54dB$ dominate.

IV. Comparison

Compared strictly on the basis of the expressions for delay resolution, mainlobe bandwidth, effective Doppler bandwidth, and peak ambiguity sidelobe presented in the previous sections, it would appear that BPC outperforms the new MSK waveform. However, a radar waveform must meet certain constraints imposed by the transmission and reception of the modulation, as well as criteria dictated by the observation. In particular, the phase discontinuity of the BPC waveform presents a significant impediment to the achievement of finer resolutions in radar measurements – a limitation that is overcome by using the continuous phase MSK waveform. This may be illustrated by considering the GSSR system.

To achieve the $400KW$ rated transmit power of the GSSR, the outputs from a pair of $250KW$ Klystron power amplifiers [3] [4] are combined to form the transmitted RF modulated signal. To avoid damaging levels of body current for modulations with a discontinuous phase [5], the phase switch rate of signals is limited to $8MHz$, and, for all signals, significant spectral content outside the passband must be limited. The GSSR spectrum allocation is to transmit a maximum of $600KW$ between $8500MHz$ and $8620MHz$ [6]. The observation requirements are dependent on the target; as an example, we consider a lunar observation that places requirements on the repetition period, the effective Doppler bandwidth, and the peak ambiguity sidelobe of the waveform. These requirements, along with those derived from the spectrum allocation and Klystron power amplifier, are:

Repetition Period	$11.6ms < T \leq 39ms$
Effective Doppler Bandwidth	$B_{D_{eff}} = 25.5Hz$
Peak Ambiguity Sidelobe	$\xi_{max} < -30dB$
Mainlobe Spectral Bandwidth	$B \leq 40MHz$
Peak Out of Band Spectrum	$S_{max} \leq -78\frac{dBc}{Hz}$
Maximum Phase Switch Rate	$8MHz$

Using these requirements to set the period and bandwidth of the candidate waveforms, the waveform characteristics are

given for the example case of GSSR lunar observations in Table I. Solutions for both BPC and MSK waveforms are determined that meet the spectrum, Klystron power amplifier, and science constraints of a GSSR lunar observation. The BPC waveform, with its discontinuous phase, is limited to the $8MHz$ maximum phase switch rate of the Klystron power amplifier, restricting its bandwidth to $16MHz$. The phase continuity of the MSK waveform and its lower out-of-band sidelobes allow a $40MHz$ bandwidth to be utilized. The increased allowable bandwidth for the MSK waveform provides a range resolution,

$$\Delta_r = \frac{\Delta_\tau c}{2},$$

of $9m$ compared to the 18.75 resolution obtained with the BPC waveform. Both waveforms exceed the $-30dB$ peak ambiguity function sidelobe necessary to handle the $30dB$ dynamic range of the lunar backscatter.

V. Conclusion

An MSK waveform for radar applications was introduced and compared to the conventionally used BPC waveform. The phase continuity and the lower fractional out-of-band power of MSK increased the allowable bandwidth compared to BPC, resulting in a factor of two increase in the range resolution of the radar. The MSK waveform was also demonstrated to have an ambiguity sidelobe structure very similar to that of BPC, where the sidelobe levels can be decreased by increasing the length of the m-sequence used in its generation. This ability to set the peak sidelobe level is advantageous as it allows the system to be configured to a variety of targets, including those with a larger dynamic range. Other conventionally used waveforms that posesses an even greater spectral efficiency than the MSK waveform, such as linear frequency modulation (LFM) and Costas frequency hopping, have a fixed peak sidelobe level that is therefore not configurable and can be exceeded by high contrast targets. Furthermore, in the case of a multistatic experiment observing a target in motion (an important class of observations for near-Earth planetary radar), self-interference from the transmitter to the receiver is mitigated by the MSK waveform; waveforms that have delay Doppler coupling, such as LFM, provide no such protection.

	BPC	MSK
Bandwidth	16MHz	40MHz
Period	16.4ms	19.7ms
Resolution	18.75m	9m
Effective Doppler Bandwidth	30.4Hz	25.4Hz
Peak Ambiguity Sidelobe	-51dB	-54dB
Peak Out-of-Band Spectrum	-78dBc/Hz	-95dBc/Hz

TABLE I
Characteristics of BPC and MSK waveforms for lunar observations.

Acknowledgment

The research described in this publication was carried out at the Jet Propulsion Laboratory, California Institute of Technology, under a contract with the National Aeronautics and Space Administration.

References

[1] Dilip V. Sarwate and Michael B. Pursley, "Crosscorrelation properties of pseudorandom and related sequences," *Proceedings of the IEEE*, vol. 68, no. 5, pp. 593–619, May 1980.

[2] Steve C. Cripps, *RF Power Amplifiers for Wireless Communications*, Artech House, Noorwood, MA, 1999.

[3] "Klystron amplifier type VKX-7864B, serial number 108R1," Test performance sheet, Communications & Power Industries, 2001.

[4] "Klystron amplifier 250-kW X-Band transmitter DSCC transmitter subsystem," JPL Detail Specification ES513821RevE, Jet Propulsion Laboratory, Pasadena, CA, 91109, USA, February 2000.

[5] Reginald A. Cormier and Albert Mizuhara, "250-kW CW klystron amplifier for planetary radar," *IEEE Transactions on Microwave Theory and Techniques*, vol. 40, no. 6, pp. 1056–1062, June 1992.

[6] "NASA97312," Government master file database, National Telecommunications and Information Administration.